Scientific paper

## 4-Bromobenzene Sulfonate Derivatives: Synthesis, Characterization, DFT and Molecular Docking Study

Meryem Evecen<sup>1,2,\*</sup>, Fatih Çelik<sup>3</sup>, Yasemin Ünver<sup>3</sup>, Halil İbrahim Güler<sup>4</sup>

<sup>1</sup> Department of Physics, Faculty of Arts and Sciences, Amasya University, 05100 Amasya, Turkey

<sup>2</sup> Department of Electric and Electronic Engineering, Faculty of Engineering, Amasya University, 05100 Amasya, Turkey

<sup>3</sup> Department of Chemistry, Faculty of Sciences, Karadeniz Technical University, 61080 Trabzon, Turkey

<sup>4</sup> Department of Molecular Biology and Genetics, Karadeniz Technical University Faculty of Science, 61080 Trabzon, Turkey

\* Corresponding author: E-mail: meryem.evecen@amasya.edu.tr

Received: 07-04-2025

#### **Abstract**

4-bromobenzenesulfonate derivatives (I and II) were prepared and characterized by FTIR and NMR spectroscopic methods and density functional theory. Acceptable deviations were found where the scaled vibrational frequencies at B3LY-P/6-311++G(d,p) were found to coincide with the experimentally observed values. Optimized molecular structures, UV-Vis and NLO properties were obtained for the compounds. The stability of the molecules arising from hyper conjugative interactions and charge delocalization has been analyzed using Natural Bond Orbital (NBO) analysis. The calculated HOMO and LUMO energies indicated that charge transfer occurred within the molecules. This study investigated the interactions between two synthesized compounds, I and II, and four receptor proteins: EGFR, VEGFR1, acetylcholinesterase, and *Leishmania infantum* trypanothione reductase. Molecular docking analysis was performed to evaluate binding energies and inhibition constants, revealing key interactions that provide insights into the therapeutic potential of the compounds.

Keywords: IR and NMR spectroscopy, 4-bromobenzenesulfonates, DFT, Molecular docking.

#### 1. Introduction

Sulfonate compounds are defined as salts or esters of sulfonic acids. These compounds contain a sulfonyl group, which consists of a sulfur atom bonded to double-bonded to two oxygen atoms and bonded to one carbon atom. In chemistry, sulfonates are typically represented by the -SO₃ group and play a significant role in various industrial and biological processes. In recent years, there has been increasing interest in the environmental impacts and biological activity potential of sulfonate compounds.<sup>2</sup> In this context, it is important to gain further insight into the ecotoxicological effects of sulfonates and their potential risks to human health, particularly with regard to industrial applications and public health concerns.3 Generally, sulfonate compounds continue to attract considerable attention for their applications in chemistry, biology, and environmental science. Sulfonates are often used as leaving groups due to their ease of synthesis, good nucleophilic

substitution properties, and favorable reaction pathways. Sulfonic acid esters also serve as intermediates in numerous synthetic transformations.<sup>4</sup> Moreover, sulfonate ester reactions are particularly important for understanding solvent effects on reactivity, non-classical carbocations, reaction mechanisms, and linear free energy relationships.<sup>5,6</sup> High-performance thermoplastics have recently garnered attention for their potential applications in the aerospace, electronics, and automotive industries. Among them, phenylene ether sulfones are well known for their excellent mechanical properties and thermal stability. To develop membrane materials with hydrophilic characteristics, it is desirable to chemically modify these polymers while preserving their physical properties. Sulfonation is a versatile method for modifying polymers, particularly aromatic polymers. It involves the introduction of sulfonic acid groups under suitable reaction conditions.<sup>7</sup> Sulfonated molecules have been shown to exhibit enhanced water solubility. Compounds bearing sulfonate groups also demonstrate increased intracellular activity.<sup>8</sup> These derivatives have shown significant anticoagulant, antitumor, and antibacterial activities.<sup>9-12</sup>

In light of the above literature, this study aimed to synthesize hybrid compounds (I and II) containing both sulfonate and Schiff base moieties. Density Functional Theory (DFT) calculations were performed for these compounds using the B3LYP/6–311++G(d,p) level of theory in order to investigate their molecular structures in detail. Additionally, the interactions of compounds I and II with four receptor proteins EGFR, VEGFR1, acetylcholinesterase, and *Leishmania infantum* trypanothione reductase were explored through molecular docking studies.

# 2. Experimental and Computational Methods

# 2. 1. Synthesis of 4-(((4-hydroxyphenyl) imino)methyl)phenyl 4-bromobenzene sulfonate (I)

4-formphenyl 4-bromobenzenesulfonate and 4-aminophenol were placed in a flask and heated in an oil bath at 160–170 °C with continuous stirring. After 1 h, the reaction mixture was cooled to room temperature. The resulting precipitate was purified using a DMSO-H<sub>2</sub>O (1:4) solvent system (Scheme 1). 93.65%- reaction yield, melting point: 147–149 °C. IR (KBr, cm<sup>-1</sup>): 3424 (OH), 3092 (=CH), 1626 (C=N), 1589, 1574 (C=C); <sup>1</sup>H NMR (400 MHz, DMSO-d<sub>6</sub>)  $\delta$ : N-C<sub>6</sub>H<sub>4</sub>.OH [6.82 (bs, 2H), 7.20 (bs, 2H)], O-C<sub>6</sub>H<sub>4</sub>.CH [7.20 (bs, 2H), 7.80-7.90 (m, 2H)], Br-C<sub>6</sub>H<sub>4</sub>.S [7.80-7.90 (m, 4H)], 8.61 (s, N=CH, 1H), 9.55 (s, OH, 1H); <sup>13</sup>C NMR (100 Hz, DMSO-d<sub>6</sub>)  $\delta$ : N-C<sub>6</sub>H<sub>4</sub>.OH [122.90 (2CH), 123.10 (2CH), 142.46 (C), 157.03 (C)], O-C<sub>6</sub>H<sub>4</sub>.CH [116.13 (2CH), 130.67 (2CH), 133.70 (C), 150.75 (C)], Br-C<sub>6</sub>H<sub>4</sub>.S [129.92 (C), 130.34 (2CH), 133.35 (2CH), 136.14 (C)], 156.05 (N=CH).

## 2. 2. 4-(((4-hydroxybutyl)imino)methyl) phenyl 4-bromobenzenesulfonate (II)

4-formphenyl 4-bromobenzenesulfonate and 4-aminobutanol were placed in a flask and heated in an oil bath at 160–170 °C with continuous stirring. After 1 h, the reaction mixture was cooled to room temperature. The precipitate was purified from DMSO-H<sub>2</sub>O (1:3). (Scheme 1). 90.65%- reaction yield, oily compound. IR (KBr, cm<sup>-1</sup>): 3303 (OH), 3091 (=CH), 1645 (C=N), 1599, 1574 (C=C); <sup>1</sup>H NMR (400 MHz, DMSO-d<sub>6</sub>) δ: 1.42-1.49 ( m, N-CH<sub>2</sub>-CH2-CH2-CH2-OH, 2H), 1.59-1.66 (m, N-CH2-CH2-CH2-CH<sub>2</sub>-OH, 2H), 3.42 (t, N-CH<sub>2</sub>-CH<sub>2</sub>-CH<sub>2</sub>-CH<sub>2</sub>-OH, 2H), 3.56 (t, N-CH<sub>2</sub>-CH<sub>2</sub>-CH<sub>2</sub>-CH<sub>2</sub>-OH, 2H), 4.41 (s, OH, 1H),O-C<sub>6</sub><u>H</u><sub>4</sub>-CH [7.14 (d, 2H), 7.88 (d, 2H)], Br-C<sub>6</sub><u>H</u><sub>4</sub>-S [7.74-7.81 (m, 4H)], 8.32 (s, N=CH, 1H), <sup>13</sup>C NMR (100 Hz, DMSO-d<sub>6</sub>)  $\delta$  :26.99 (N-CH<sub>2</sub>-CH<sub>2</sub>-CH<sub>2</sub>-CH<sub>2</sub>-OH), 31.07 (N-CH<sub>2</sub>-CH<sub>2</sub>-CH<sub>2</sub>-CH<sub>2</sub>-OH), 60.73 (N-<u>C</u>H<sub>2</sub>-CH<sub>2</sub>- $CH_2$ - $CH_2$ -OH), 60.88 (N- $CH_2$ - $CH_2$ - $CH_2$ - $CH_2$ -OH),  $O-\underline{C}_6H_4$ -CH [122.89 (2CH), 130.64 (2CH), 133.96 (C), 150.73 (C)], Br-<u>C</u><sub>6</sub>H<sub>4-</sub>S [129.79 (2CH), 133.48 (2CH), 135.87 (2C)], 159.62 (N=CH).

#### 2. 3. Chemistry

The characteristic vibrational bands of the carbonyl (C=O) and amine (NH<sub>2</sub>) groups present in the starting materials were not observed in the IR spectra of compounds I and II, confirming their conversion during synthesis. The <sup>1</sup>H NMR spectra showed imine (– CH=N) proton signals at 8.61 and 8.32 ppm for compounds I and II, respectively. The corresponding <sup>13</sup>C NMR signals of the imine carbon were detected at 156.05 and 159.62 ppm. Additionally, aromatic proton and carbon signals appeared in the expected chemical shift regions, further supporting the proposed structures.

Scheme 1. Synthetic pathway of compounds I-II.

#### 2. 4. Computantial Method

All DFT calculations of compounds I and II were performed with the DFT/B3LYP method and 6–311++ G (d,p) basis set in the Gaussian 09<sup>13</sup> package program. The GaussView<sup>14</sup> program was used to visualize the results obtained from the calculations. A scale factor of 0.96 was used to align the calculated vibration frequencies with the experimental ones. The GIAO<sup>15,16</sup> approach was used for chemical shift calculations of the two molecules. The chemical shifts for <sup>1</sup>H and <sup>13</sup>C were determined using scale factors of 31.965 and 184.655 ppm, respectively.

#### 3. Results and Discussion

#### 3. 1. Optimized structure

Structural information is essential when investigating the coordination properties of Schiff bases acting as ligands. Herein, we report the predicted molecular structures of compounds I and II, determined with DFT quantum-chemical calculations (B3LYP / 6–311++ G(d,p)), as well as some structural information derived from them using the VESTA program. The initial geometries of the molecules were defined in an ab initio manner using GaussView; the atom numbering scheme is illustrated in Figure 1. The chemical formula of compound I is  $C_{19}H_{14}BrNO_4S$ , with a molecular weight of 432 g/mol, while the chemical formula of compound II is  $C_{17}H_{18}BrNO_4S$ , with a molecular weight of 412 g/mol. Both compounds are anticipated to crystallize in the triclinic crystal system (despite several attempts, we could

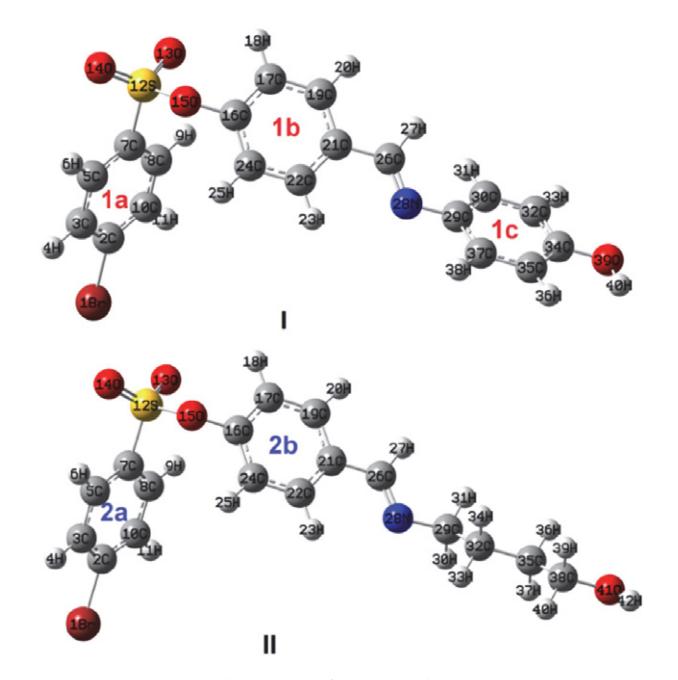


Figure 1. Optimized structure of compounds, (I) and (II).

not reliably determine the structures of the above compounds experimentally). The comparative optimized structural parameters are summarized in Table 1. Theoretically based on the calculated values, all C–C bond lengths in the benzene rings exhibit slight variations.

Therefore, the hexagonal structure of benzene rings is not affected by SO<sub>3</sub> interaction. The bond length of S=O cal-

 $\textbf{Table 1.} \ Selected \ molecular \ structure \ parameters \ of the \ compounds \ I \ and \ II.$ 

Bond length	Theor. I/II	Exp.(Ia /IIb )	Bond length	Theor. I/II	Exp.(Ia /IIb )
Br1-C2	1.911 / 1.911	1.890(3) / 1.911	C26-N28	1.277 / 1.269	1.270(3) / 1.269
C7-S12	1.789 / 1.789	1.751(3) / -	N28-C29	1.405 / 1.453	1.390(3) / 1.452
S12=O13	1.454 / 1.454	1.419(3) / 1.453	C34-O39	1.369 / -	-/-
S12=O14	1.447 / 1.447	1.412(3) / 1.453	C29-C32	- / 1.533	- / 1.534
S12-O15	1.673 / 1.673	1.594(2) / 1.672	C32-C35	- / 1.532	- / 1.533
O15-C16	1.397 / 1.398	1.420(3) / 1.398	C35-C38	- / 1.521	- / 1.533
C21-C26	1.468 / 1.474	- / 1.424	C38-O41	- / 1.430	-/-
Bond angles					
Br1-C2-C3	119.180 / 119.174	120.0 (2) / -	C26-N28-C29	120.902 / 118.498	121.9 (2) / 118.6
S12-O15-C16	121.267 / 121.036	119.49 (18) / 117.9	C35-C34-O39	122.793 / -	-/-
O13-S12-O14	122.395 / 122.428	121.47 (17) / 120.9	N28-C29-C32	- / 111.120	- / 110.7
O14-S12-O15	102.935 / 102.998	102.68 (16) / -	C29-C32-C35	- / 112.391	- / 113.0
C7-S12-O15	102.669 / 102.701	103.86 (13) / 96.6	C32-C35-C38	- / 112.671	- / 111.5
C21-C26-N28	122.594 / 123.241	120.1 (3) / 123.0	C35-C38-O41	- / 108.030	-/-
Torsion angles					
Br1-C2-C3-C5	-179.888 / -179.952	-177.5 (3) / -	C26-N28-C29-C30	-33.913 / -	-/-
C7-S12-O15-C16	73.297 / 74.700	-78.6 (2) / 179.80	C26-N28-C29-C32	- / 123.443	- / 123.95
O13-S12-O15-C16	-41.836 / -40.422	37.5 (2) / -	N28-C29-C32-C35	- / 176.568	- / 176.50
S12-O15-C16-C17	70.374 / 71.647	93.0 (3) / -	C29-C32-C35-C38	- / -179.860	- / -179.65
C21-C26-N28-C29	177.406 / -179.978	176.4 (2) / -179.69	C32-C35-C38-O41	- / -179.757	-/-

Ia: Ref. [22]; IIb: Ref. [23]

culated by DFT is 1.454 Å and 1.447 Å, respectively. On comparing these values with the experimental values of 1.419 Å and 1.412 Å, respectively. It is known that the DFT overestimates the bond length. <sup>18,19</sup> The calculated bond value of 1.789 for C–S is in agreement with the experimental values in the literature. <sup>20</sup> The bond lengths of Br1–C2, O15=C16, and C26=N28 are 1.911 (1.911), 1.397 (1.398) and 1.277 (1.269) Å in the structures of compound I (compound II). Compound I has three benzene rings in its molecular structure. Compound II has two benzene rings and alkyl groups. Phenyl 4-bromo benzene sulfonate is included in the molecular structure of both compounds (Figure 1).

In the molecular structure of compound II, the alkyl group is bonded to the N28 atom. The replacement of the benzene ring in compound I with the alkyl group in com-

pound II was effective in changing the dihedral angles in the phenyl 4-bromobenzenesulfonate part. It causes C7-S12-O15-C16 dihedral angle to change by 1.5°. The values of other bond lengths and angles of the molecules are given in Table 1. It can be seen from Table 2 that calculated bond length, bond angles and torsion angles are within normal ranges and in agreement with each other and other experimental and theoretical values. 21-23

#### 3. 2. Spectroscopic Properties

#### Vibrational Spectra

The IR spectral data for compounds I and II were obtained at DFT/B3LYP/6-311++G(d,p) level and are presented in Figure 2. To improve the agreement between the-

**Table 2.** Some of calculated and experimental vibrational frequencies (cm<sup>-1</sup>).

	I			II	
Assignments	Exp.	Theo.	<b>Assignments</b> a	Exp.	Theo.
ν (OH) s	3424	3682	ν (OH) s	3303	3690
ν (CH) s 1a	3092	3084	ν (CH) s 2a	3091	3084
ν (CH) al		2887	ν (CH) s 2b		3075
ν (C=N) s	1626	1616	ν (CH) as 2a		3070
v (CC) 1b,1c + $v$ (C=N)	1589	1580	ν (CH) as 2b		3062
$v$ (CC) 1c + $\gamma$ (OH)	1574	1553	$\nu$ (CH <sub>2</sub> ) as	2935	2949
v (CC) 1b + $v$ (C=N)	1506	1545	$\nu (CH_2)$ s		2907
γ (CH) 1b,1c	1472	1475	ν (CH) al	2858	2850
γ (CH) 1a	1448	1440	v (C=N) s	1645	1645
γ (OH)+ γ (CH)1c	1391	1404	v (CC) $2b + v$ (C=N)	1599	1549
γ (CH) al	1372	1384	ν (CC) 2a	1574	1543
ν (OSO) as	1298	1292	$\alpha$ (CH <sub>2</sub> )	1499	1464
ν (CCC) 1a	1282	1262	γ (CH) 2a	1472	1440
ν (C-OH)	1233	1230	$\gamma$ (OH)+ $\gamma$ (CH <sub>2</sub> )	1391	1393
$\nu$ (C-N)+ $\nu$ (CH)al	1195	1212	γ (CH) al	1374	1385
ν (C-N)+ ν (CO)	1166	1164	ν (OSO) as	1297	1292
$\alpha$ (CH) 1c+ $\alpha$ (OH)	1144	1140	ν (CCC) 2a	1280	1261
v (CSO <sub>2</sub> ) as	1091	1095	$\delta (CH_2) + \nu (OH)$	1197	1232
Q (CCC) 1a	1066	1032	v (CC=N) + v (CH)al	1172	1192
β (CCC)1b, 1c	1010	989	$\omega$ (CH <sub>2</sub> ) 2c + $\nu$ (OH)	1148	1177
$\nu$ (B-C)+ $\beta$ (CCC)1a	970	982	$\delta$ (CH <sub>2</sub> )	1148	1164
δ (CH) 1a	945	931	$\nu$ (CSO <sub>2</sub> ) as	1089	1095
Q (CCC) 1b, 1c	865	861	Q (CCC) 2a	1067	1032
ω (CH) 2b	843	832	$\nu$ (N-CH <sub>2</sub> )+ $\nu$ (C-OH)	1010	1011
ν (CO)+ Q (CCC) 1b	828	828	$\nu$ (B-C)+ $\beta$ (CCC)2a		982
$\omega$ (CH) 1c + $\nu$ (CO)	819	810	δ (CH) 2a		931
ω (CH) 1b	786	806	ν (CO)+ Q (CCC) 2b	854	841
ω (CH) 1a	760	800	$\omega$ (CH) 2b + $\nu$ (CO)	822	828
$\nu$ (CO)+ $\nu$ (CN)	732	757	$v$ (CO)+ $\omega$ (CH <sub>2</sub> )	751	799
$\beta(CCC)1a+\nu(B-C)+\tau(CCC)1b$	714	719	$\beta$ (CCC) 2a+ $\nu$ (B-C)	731	717
τ (CCC) 1c	707	692	τ (CCC) 2b	708	711
τ (CCC) 1a	634	686	τ (CCC) 2a	647	689
ν (OS)	627	637	v (OS)	637	642
β (CCC) 1b	621	622	β (CCC) 2b	621	626
ν (SO)	592	596	ν (SO)	598	600
ν (CS)	563	561	ν (CS)	563	561

 $<sup>\</sup>alpha$  v, stretching; α, scissoring; γ, rocking; ω, wagging; δ, twisting; β, bending; τ, torsion; Q, breathing; s, symmetric; as, asymmetric; al, alifatic. Abbreviations: 1a,1b,1c, 2a,2b, rings.

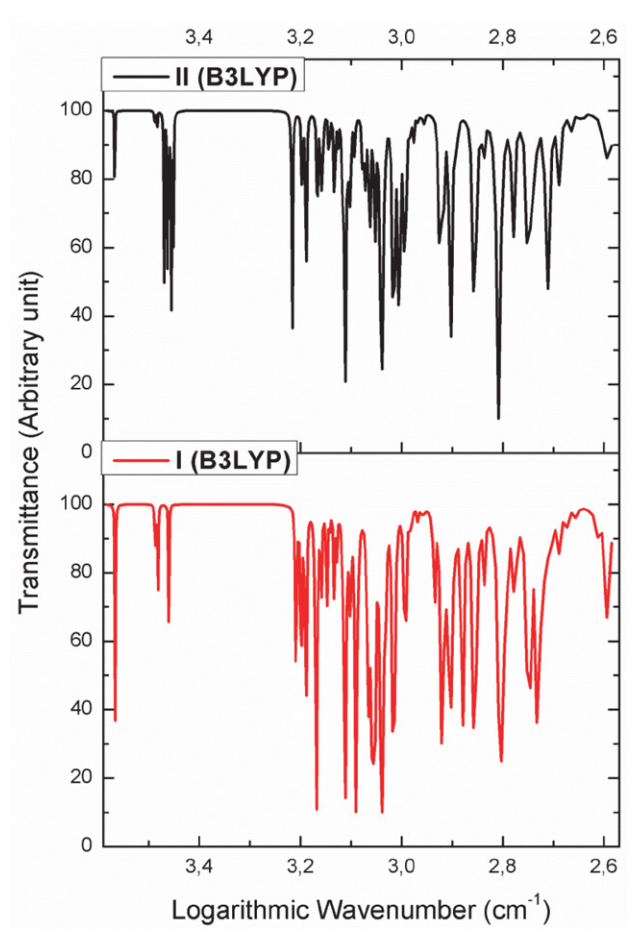


**Figure 2.** Calculated IR spectra of compounds I and II (for the experimental spectra, see Figures S1 and S2). (Note: Logarithmic wavenumbers 3.4, 3.2, 3.0, 2.8 and 2.6 correspond wavenumbers 2511, 1585, 1000, 630 and 398, respectively).

oretical and experimental frequencies, the calculated theoretical frequencies were scaled by a factor of 0.96.<sup>24</sup> Experimental and calculated vibration frequencies values of the compounds are compared in Table 2. The vibrational bands corresponding to the carbonyl (C=O) and amine (NH<sub>2</sub>) groups of the starting materials were not observed in the IR spectra of compounds I and II, confirming their conversion during the synthesis.

As shown in Table 2, the theoretical IR data corroborate the molecular structures of compounds I and II. The free hydroxyl group absorbs strongly in the region 3700–3584 cm<sup>-1</sup>.<sup>25</sup> In the present study, a strong O-H vibration was observed at 3682 (3424) cm<sup>-1</sup> for compound I and 3690 (3303) cm<sup>-1</sup> for compound II in theoretical IR (experimental FT-IR) result. For both compounds, the C-H stretching vibrations at 3092 and 3091 cm<sup>-1</sup> correspond to the characteristic FT-IR absorption bands of aromatic benzene rings, in good agreement with the calculated values.

For compounds I and II, the calculated N=C stretching bands at 1616 and 1645 cm<sup>-1</sup> at the B3LYP level were observed as 1626 and 1645 cm<sup>-1</sup> in the FT-IR spectra, re-

spectively. These stretching mode is also supported by the similiar literatüre reports.  $^{26,23}$  The asymmetric SO $_2$  stretching vibrations ocur in the region 1295–1330 cm $^{-1}$ . In our molecules, the calculated SO stretching vibration appears at 1292 cm $^{-1}$ , in good agreement with the literature.  $^{28-30}$  Other vibrational frequencies can be found in Table 2 and Figures S1 and S2.

#### NMR studies

<sup>1</sup>H and <sup>13</sup>C NMR chemical shift values of (I) and (II) molecules were obtained using the B3LY-P/6-311++G(d,p) method, employing the GIAO-NMR approach in DMSO solvent media, and compared with the experimental values (Table 3). The experimental spectra are presented in Figures S3-S6 (see Supplementary information). In agreement with the experimental data, the <sup>1</sup>H NMR signals of the imine group (N=CH) appeared at 8.93 and 8.73 ppm for compounds I and II, respectively. The <sup>13</sup>C NMR signals of the imine group (CH=N) were calculated at 163.94 and 166.85 ppm and observed experimentally at 156.05 and 159.62 ppm. The aromatic carbon chemical shift of compound I (compound II) are consistent with the ranges of 116.13-157.03 ppm (130.05<sup>-</sup>162.32 ppm), corresponding to the aromatic ring carbons, while the aromatic proton signals are in agreement with the ranges of 6.82-7.90 ppm (6.83-8.40 ppm). The <sup>1</sup>H and <sup>13</sup>C signals of the aromatic rings were observed in the expected regions, consistent with the calculated values. Additionally, the 13C (1H) signals of the alkyl groups in compound I were observed at 60.73, 26.99, 31.07, and 60.88 ppm (1.18-4.06 ppm) and calculated at 70.23, 33.43, 35.09, and 70.00 ppm (1.42-3.56 ppm), respectively. Similarly, the O-H signals for compounds I and II were observed at 9.55 and 4.41 ppm and calculated at 4.60 and 0.92 ppm, respectively. The contents of Table 3 are presented as a correlation plot in Figures S7 and S8. Therefore, it can be concluded that the experimental and calculated NMR data for both compounds are in good agreement.

#### **UV** studies

UV-Vis spectra of the molecules (I and II) were calculated at B3LYP level using the 6-311G ++(d, p) base set, according to the Time Dependent (TD) DFT methodology. In order to include solvent effects, the implicit IEFPCM model was adopted. The results are listed in Table 4. The GaussSum program<sup>31</sup> was used to show the important transitions. Three main peaks were observed in both methods (Figure 3). Table 4 for (I) in gas shows the wavelengths 288 and 370 nm with oscillator strengths, i.e., 0.366 and 0.474 respectively, which indicate relatively stronger allowed transitions. Wavelengths of 249 nm with a low magnitude of oscillator strength (0.052) show weak transitions.

For compound II in DMSO solvent, Table 4 shows the wavelengths as 289 and 374 nm with oscillator

Table 3. Theoretical and experimental <sup>1</sup>H- and <sup>13</sup>C NMR data for compounds I and II.

	I		II	
Atom	Exp.	Calculated (in DMSO)	Exp.	Calculated (in DMSO)
C2,C3,C5,C7, C8,C10	136.14, 133.35, 130.34, 129.92, 130.34, 133.35	157.60, 140.88, 135.97, 146.49, 135.77, 139.52	135.87, 133.48, 129.79, 135.87, 129.79, 133.48	157.51, 140.80, 135.91, 146.33, 135.84, 139.68
C16,C17,C19,C21, C22,C24	150.75, 116.13, 130.67, 133.70, 130.67, 116.13	161.35, 131.54, 141.34, 144.26, 133.93, 130.29	150.73, 122.89, 130.64, 133.96, 130.64, 122.89	161.32, 131.85, 140.08, 143.75, 133.34, 130.05
C26	156.05	163.94	159.62	166.85
C29,C30,C32,C34, C35,C37 C29(II), C32(II),C35(II),C38 (II)	142.46, 123.10, 122.90, 157.03, 122.90, 123.10	153.03, 124.56, 121.98, 164.82, 120.08, 134.54	60.73, 26.99, 31.07, 60.88	70.23, 33.43, 35.09, 70.00
H4,H6,H9,H11	7.90, 7.90, 7.80, 7.80	8.00, 8.14, 7.38, 7.64	7.81, 7.81, 7.74, 7.74	8, 00, 8.15, 7.28, 7.67
H18,H20,H23,H25	7.20, 7.80, 7.90, 7.20	7.89, 8.02, 8.43, 6.91	7.88, 7.14, 7.88, 7.14	7.82, 7.70, 8.40, 6.83
H27	8.61	8.93	8.32	8.75
H31,H33,H36,H38 H30(II), H31 (II)	7.20, 6.82, 6.82, 7.20	7.48, 7.21, 7.07, 7.50	3.42, 3.42	4.06, 3.39
H33(II), H34 (II)			1.49, 1.42	1.90, 1.18
H36(II), H37 (II)			1.66, 1.59	1.70, 1.68
H39(II), H40 (II) H40 H42 (II)	9.55	4.60	3.56 4.41	3.80, 3.87 0.91

strengths, i.e., 0.351 and 0.615, respectively, which indicate relatively stronger allowed transitions. The wavelengths at 249 nm with a low magnitude of oscillator strength, i.e., 0.032, are characterized by weak transitions. Compound II oscillator strength at all wavelengths in both gas and DMSO media shows relatively strong allowed transitions.

### 3. 3. Electronic Properties

#### Molecular orbital calculations

The highest occupied molecular orbital (HOMO) and the lowest unoccupied molecular orbital (LUMO) are the fundamental orbitals that participate in chemical reactions. These are also referred to as frontier molecular orbitals (FMOs). Boundary value orbital analysis is as im-

Table 4. Calculated and experimental absorption wavelength, oscillator strengths and energies of compounds I and II

Gas							DMSO			
Trans.	E (eV)	f	λ (nm)	*Contribution (H-1, H, L, L+1)	E (eV)	f	λ (nm)	*Contribution (H-1, H, L, L+1)		
(I)										
1	3.35	0.474	370	H→L (91%), H→L+1 (4%)	3.32	0.615	374	H→L (94%), H→L+1 (2%)		
2	4.30	0.366	288	H-1→L (59%), H-1→L+1 (5%), H→L (2%), H→L+1 (3%)	4.30	0.351	289	H-1→L (61%), H→L+1 (2%)		
3	4.97	0.052	249	-	4.99	0.032	249	_		
(II)										
1	4.31	0.180	288	H→L (96%), H→L+1 (3%)	4.37	0.352	284	H→L (96%), H→L+1 (2%)		
2	4.71	0.206	263	H→L+1 (39%)	4.80	0.209	259	H→L+1 (44%)		
3	5.86	0.184	212	-	5.81	0.290	213	_		

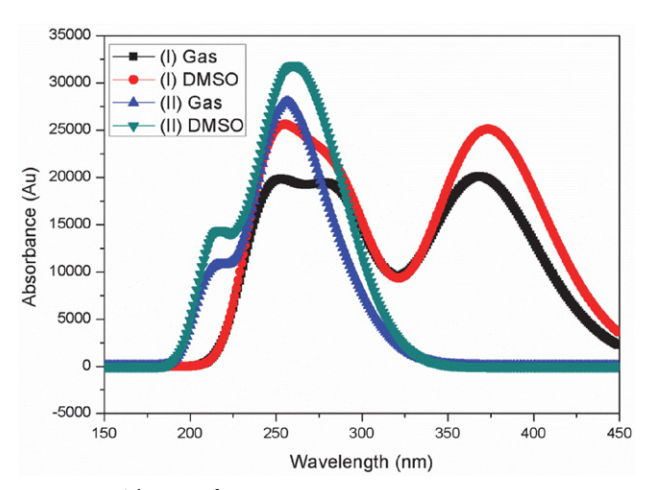


Figure 3. Theoretical UV-Vis spectras.

portant as chemical reactions in determining electrical and electronic properties. The energies of HOMO and LU-MO are negative, which indicates the stability of compounds.<sup>32</sup>

The breakpoint orbital analysis of both molecules was performed using the B3LYP/6-311++G(d,P) method. The orbital values of compound I (compound II) as LU-MO+1, LUMO, HOMO and HOMO-1 were calculated as -1.99~(-1.81),~-2.24~(-2.14),~-6.03~(-6.96) and -7.22~(-7.35) eV. The energy diagrams were visualized in Figure 4. The energy gap ( $\Delta$ E) between the frontier molecular orbitals is an important parameter in determining the chemical reactivity of a molecule, which can influence properties such as electronegativity, chemical hardness, and softness. Molecules with a high chemical hardness value

**Table 5**. Energy gap ( $\Delta E$ ), electron affinity ( $\Upsilon$ ), ionization potential (I), absolute electronegativity ( $\Phi$ ), chemical hardness ( $\Psi$ ), absolute softness (S) and electrophilic index ( $\omega$ ) parameters calculated at B3LYP/6-311G++(d,p).

Quantum chemical parameters (eV)	(I)	(II)
$\Delta E = E_{LUMO} - E_{HOMO}$	3.79	4.82
$\Upsilon = -E_{LUMO}$	2.24	2.14
$I = -E_{HOMO}$	6.03	6.96
$\phi = \frac{Y + I}{2}$	4.14	4.55
$\Psi = \frac{l - Y}{2}$	1.89	2.41
$S = \frac{1}{\Psi}$	0.53	0.42
$S = \frac{1}{\Psi}$	4.53	4.29

have a large energy range, while softer molecules have a smaller one. Table 5 shows that ionization potential (I), electron affinity (Y), absolute electronegativity ( $\Phi$ ), chemical hardness ( $\Psi$ ), absolute softness (S), and electrophilic index ( $\omega$ ) parameters are given for molecules. These values are compatible with the charge distribution in Figure 4. Adding 4-hydroxybutyl to molecule (II) in place of 4-hydroxyphenyl in molecule (I) increased the energy gap ( $\Delta$ E). Therefore, the electronegativity of (II) molecules is greater than molecules (I).

#### **MEP Analysis**

The Molecular Electrostatic Potential (MEP) surface provides important information such as potential sites for nucleophilic or electrophilic attack and the reactive regions of a molecule.<sup>33</sup> The MEP contour plot is related to

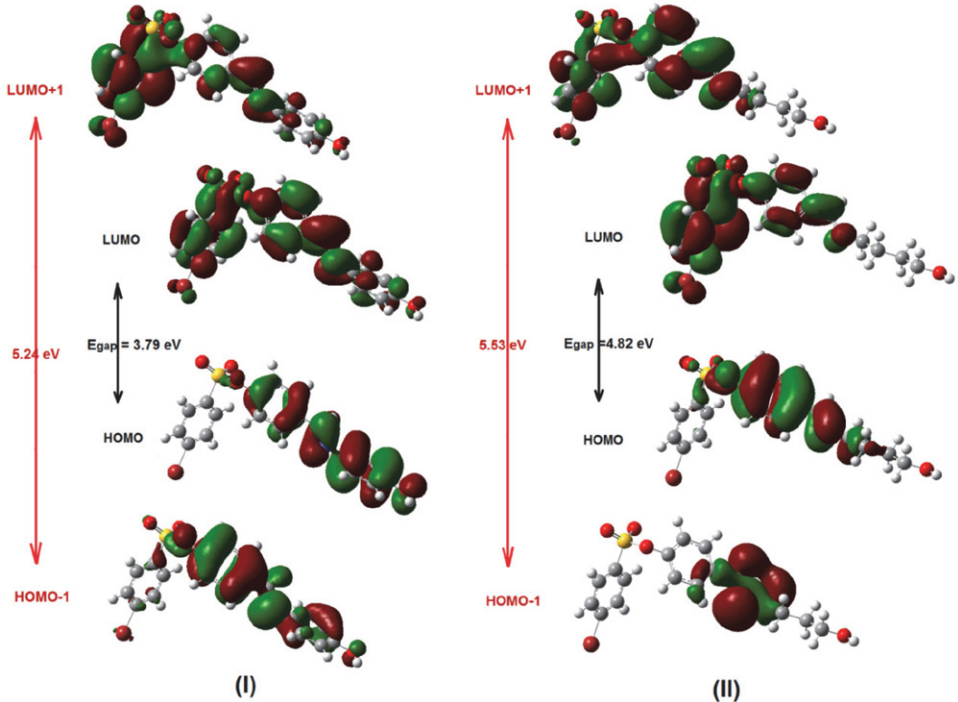


Figure 4. Frontier molecular orbitals for compounds I and II.

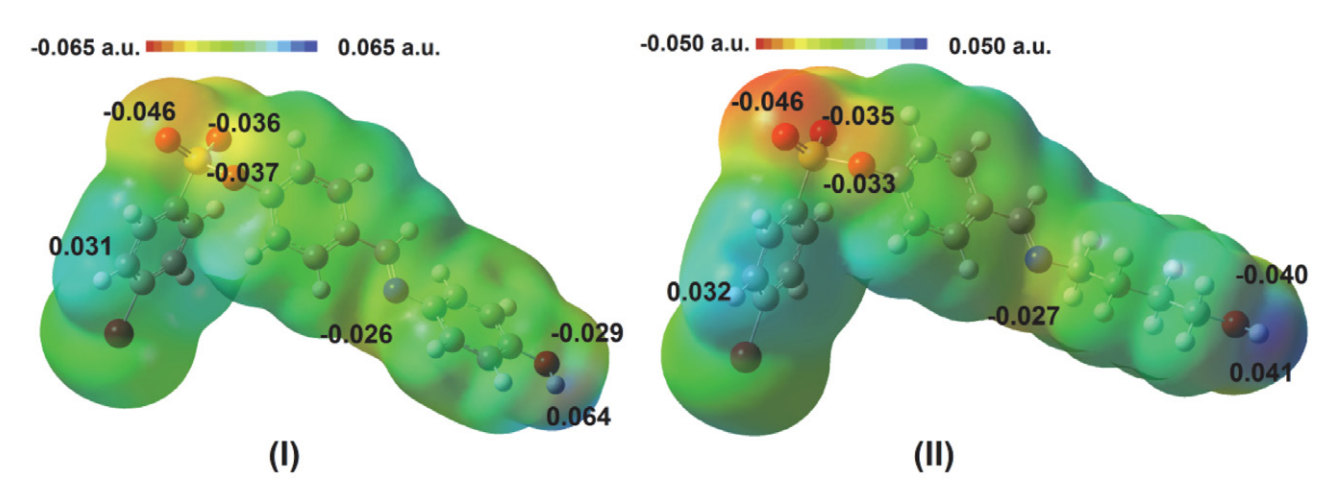


Figure 5. MEP surfaces of compounds.

the relative electron density. The different values of the electrostatic potential at the surface are represented by different colors. Potential increases in the order red < orange

< yellow< green < blue. Blue shows the strongest attraction and red shows the strongest repulsion in the color code. Regions of negative V(r) are usually associated with the

**Table 6.** Selected second-order perturbation energies  $E^{(2)}$  associated with  $i \rightarrow j$  delocalization in gas phase.

Donor orbital (i)	Type	ED/e	Acceptor orbital (j)	Type	ED/e	E <sup>(2)</sup> (kcal/mol) <sup>a</sup>	E(j)-E(i) (a.u.) <sup>b</sup>	F(i,j) (a.u.) <sup>c</sup>
(I)								
C2-C10	π	1.66097	C7-C8	π*	0.38681	21.88	0.28	0.071
C3-C5	π	1.64640	C2-C10	$\pi^*$	0.37102	22.32	0.27	0.070
C7-C8	π	1.68533	C3-C5	$\pi^*$	0.29130	21.48	0.30	0.072
C19-C21	π	1.62875	C16-C17	π*	0.36887	20.93	0.27	0.067
C22-C24	π	1.67302	C16-C17	π*	0.36887	21.81	0.28	0.070
C29-C37	π	1.62630	C30-C32	$\pi^*$	0.33140	21.18	0.28	0.069
C30-C32	π	1.71244	C34-C35	$\pi^*$	0.39797	21.36	0.28	0.071
C34-C35	π	1.64883	C29-C37	$\pi^*$	0.38635	22.31	0.29	0.073
LP (3)-O13		1.76205	S12-O15	$\sigma^*$	0.35060	32.85	0.35	0.098
LP (3)-O14		1.76306	S12-O15	$\sigma^*$	0.35060	30.46	0.34	0.094
LP (2)-O39		1.87788	C34-C35	$\sigma^*$	0.02711	27.20	0.35	0.094
C2-C10	π	1.66097	C3-C5	$\pi^*$	0.29130	200.14	0.01	0.080
C7-C8	π	1.68533	C3-C5	$\pi^*$	0.29130	203.80	0.01	0.000
C16-C17	π	1.65254	S12-O15	$\sigma^*$	0.35060	34.55	0.02	0.041
C16-C17	π	1.65254	C22-C24	$\pi^*$	0.28641	238.73	0.01	0.080
C34-C35	π	1.64883	C29-C37	$\pi^*$	0.38635	295.91	0.01	0.081
(II)								
C2-C10	π	1.66093	C7-C8	π*	0.38699	21.88	0.28	0.071
C3-C5	π	1.64598	C2-C10	$\pi^*$	0.37152	22.34	0.27	0.070
C7-C8	π	1.68488	C3-C5	$\pi^*$	0.29169	21.50	0.30	0.072
C19-C21	π	1.63478	C16-C17	$\pi^*$	0.36718	20.94	0.27	0.068
C22-C24	π	1.67108	C16-C17	$\pi^*$	0.36718	21.88	0.28	0.070
LP (3)-O13		1.76174	S12-O15	$\sigma^*$	0.35058	32.86	0.35	0.098
LP (3)-O14		1.76329	S12-O15	$\sigma^*$	0.35058	30.35	0.34	0.094
C2-C10	π	1.66093	C3-C5	$\pi^*$	0.29169	198.88	0.01	0.080
C7-C8	π	1.68488	C3-C5	$\pi^*$	0.29169	203.42	0.01	0.080
C16-C17	π	1.65460	S12-O15	$\sigma^*$	0.35058	35.23	0.02	0.041
C16-C17	π	1.65460	C22-C24	$\pi^*$	0.28931	249.80	0.01	0.080

 $<sup>^</sup>a$ E(2), energy of hyper conjugative interactions.  $^b$  Energy difference between donor and acceptor i and j NBO orbitals.  $^cF_{ij}$  is the Fock matrix element between i and j NBO orbitals.

lone pair of electronegative atoms. According to Figure 5, the electron-rich centres were found around the O atoms and slightly around the N atoms (red region). Hydrogen atoms had the strongest attraction while N and O atoms had the strongest repulsion (blue region).

#### **NBO** Analysis

Natural Bond Orbitals (NBO) analysis provides insights into the electron density distribution across the orbitals.<sup>34</sup> The stabilization energy  $E^{(2)}$  related to delocalization from I (donor) to j (acceptor) is given by.<sup>35,36</sup>

$$E^{(2)} = -q_i \frac{(F_{ij})^2}{\varepsilon_j - \varepsilon_i}$$

where  $q_i$  is the donor orbital occupancy,  $\varepsilon_i$ ,  $\varepsilon_i$  are diagonal elements (orbital energies) and  $E_{ii}$  is the off-diagonal NBO Fock matrix element. The interaction stabilization energy  $(E^2)$  and donor and acceptor electron orbitals are tabulated. The electron densities of the donor and acceptor NBO orbitals are denoted by ED/e. The compounds include three different forms of transitions such as  $\pi \to \sigma^*$ ,  $\pi \to \pi^*$ and LP  $\rightarrow \sigma^*$ . For Table 6, stabilization energies greater than 20 kcalmol<sup>-1</sup> have been chosen. A high  $E^{(2)}$  value indicates that the interaction between electron donors and acceptors is strong. The NBO analysis has been performed on the molecule at the B3LYP/6311 G++ (d,p) level in order to elucidate the intramolecular, rehybridization and delocalization of electron density within the molecule. The strong intramolecular hyper-conjugative interactions are formed by the orbital overlap between bonding (C-C) and anti bonding (C-C) and (S-O) orbitals, which result in Intramolecular Charge Transfer (ICT) causing stabilization of the molecular system.

These interactions are observed as an increase in Electron Density (ED) in the (C-C) and (S-O) anti bonding orbitals, which weakens the respective bonds. In compound I, the  $\pi$  electron delocalization is maximum around C34-C35, distributed into  $\pi^*$  anti bonding of C29-C37 with the stabilization energy 295.91 kJ/mol. In both mole-

cules,  $\pi$  electron delocalization is maximum around C2-C10, C7-C8 and C16-C17. If  $\pi^*$  anti-binding is distributed in the C3-C5 and C22-C24 regions. Other parameters related to stabilization energy are shown in Table 6.

#### **NLO Properties**

Molecules with NonLinear Optical (NLO) properties have been extensively studied because of their wide application in data storage technology, telecommunications, signal processing, laser technology, optical communication and optical interconnections. The NLO properties of materials are well predicted with computer aid using existing theoretical methods. The calculations of the dipole moment ( $\mu$ ), polarizability ( $\alpha$ ) and hyperpolarizability ( $\beta$ ) from the Gaussian output have been explained in detail.<sup>37</sup>

The first hyperpolarizability is a third rank tensor that can be described by a  $3\times3\times3$  matrix. The 27 components of the matrix can be reduced to 10 components due to Kleinman symmetry.<sup>38</sup> The complete equations for calculating the magnitude of the first hyperpolarizability  $\beta_T$ , using the x,y,z components are as follows:

$$\beta_{x} = \beta_{xxx} + \beta_{xyy} + \beta_{xzz}$$

$$\beta_{y} = \beta_{yyy} + \beta_{xxy} + \beta_{yzz}$$

$$\beta_{z} = \beta_{zzz} + \beta_{xxz} + \beta_{yyz}$$

$$\beta_{z} = \beta_{zzz} + \beta_{xxz} + \beta_{yyz}$$

 $\mu,\alpha$  and  $\beta$  values of the title compound are listed in Table 7. Urea  $(\mu,\alpha$  and  $\beta$  value were 3.88 D, 5.04 Å  $^3$  and 0.782  $\times$   $10^{-30}$  cm  $^5$ /esu obtained by B3LYP/6-311++G(d,p) method) is one of the prototypical molecules to compare NLO properties of the organic molecular systems, respectively. The calculated  $\beta$  values were found to be nearly 46.96 times for the I molecule and 3.5 times for the II molecule in B3LYP. Both compounds I and II have values greater than that of urea.

According to the the magnitude of molecular hyperpolarizability, studied compounds are good candidate as NLO materials.

Table 7. The dipole moment.	polaricability	and firet hyr	ornolarizability	v21110c
Table 7. The dibole moment.	polarisability	and first flyt	erpolarizability	varues

	(I)B3LYP	(II)B3LYP		(I)B3LYP	(II)B3LYP
Dipol			HyperPola	ır	
$\mu_x$	2.3559	1.8456	$\beta_{xxx}$	-3658.95	-201.10
$\mu_{y}$	3.3650	2.7291	$\beta_{xxy}$	1111.44	-93.59
$\mu_z$	-0.7865	-0.7354	$\beta_{xyy}$	-351.64	140.29
$\mu_{\mathrm{T}}$	4.1823	3.3756	$\beta_{yyy}$	509.28	321.65
Polar			$\beta_{xxz}$	29.60	-200.99
$\alpha_{xx}$	440.10	343.04	$\dot{eta}_{ m xyz}$	-95.83	16.55
$a_{xy}$	-53.26	-13.36	$\beta_{yyz}$	5.23	-32.52
$\alpha_{yy}$	293.38	287.39	$\beta_{xzz}$	52.62	68.55
$\alpha_{xz}$	-25.45	-29.30	$\beta_{yzz}$	-73.07	-51.92
$\alpha_{yz}$	-17.77	-8.28	$\beta_{zzz}$	26.25	-29.83
$\alpha_{zz}$	222.38	202.20	$\beta_{\rm T}$	$36.726 \times 10^{-29}$	$2.7384 \times 10^{-30}$
$a_{\mathrm{T}}$	47.17	41.09			

#### 3. 4. Molecular Docking Study

Molecular docking is an essential tool in drug discovery, enabling researchers to efficiently assess potential drug candidates by predicting their interactions with target proteins. This computational technique not only accelerates the screening process but also minimizes the time and cost required for traditional experimental methods.<sup>39-41</sup> In this study, docking analyses were performed to investigate the binding interactions of newly synthesized compounds, I and II, with four key receptor proteins: Epidermal Growth Factor Receptor (EGFR), Vascular Endothelial Growth Factor Receptor 1 (VEGFR1), Human Acetylcholinesterase (AChE), and Trypanothione Reductase from Leishmania infantum. The 3D structures of EG-FR (PDB ID: 1M17) and VEGFR1 (PDB ID: 3HNG) used in this study have also been employed in similar docking analyses reported in the literature, as demonstrated in studies on diverse cancer-targeting ligands. 42,43,23

EGFR, a transmembrane protein critical for cellular signaling pathways, is commonly targeted in cancer therapies, as mutations affecting its activity are implicated in various cancers by promoting cell proliferation and survival. 44 VEGFR1, meanwhile, plays a crucial role in angiogenesis by regulating blood vessel formation, which is particularly important in cancer research, as inhibiting this receptor can disrupt the tumor's blood supply. 45 Effective inhibition of these receptors provides strategic targets for anti-cancer therapies.

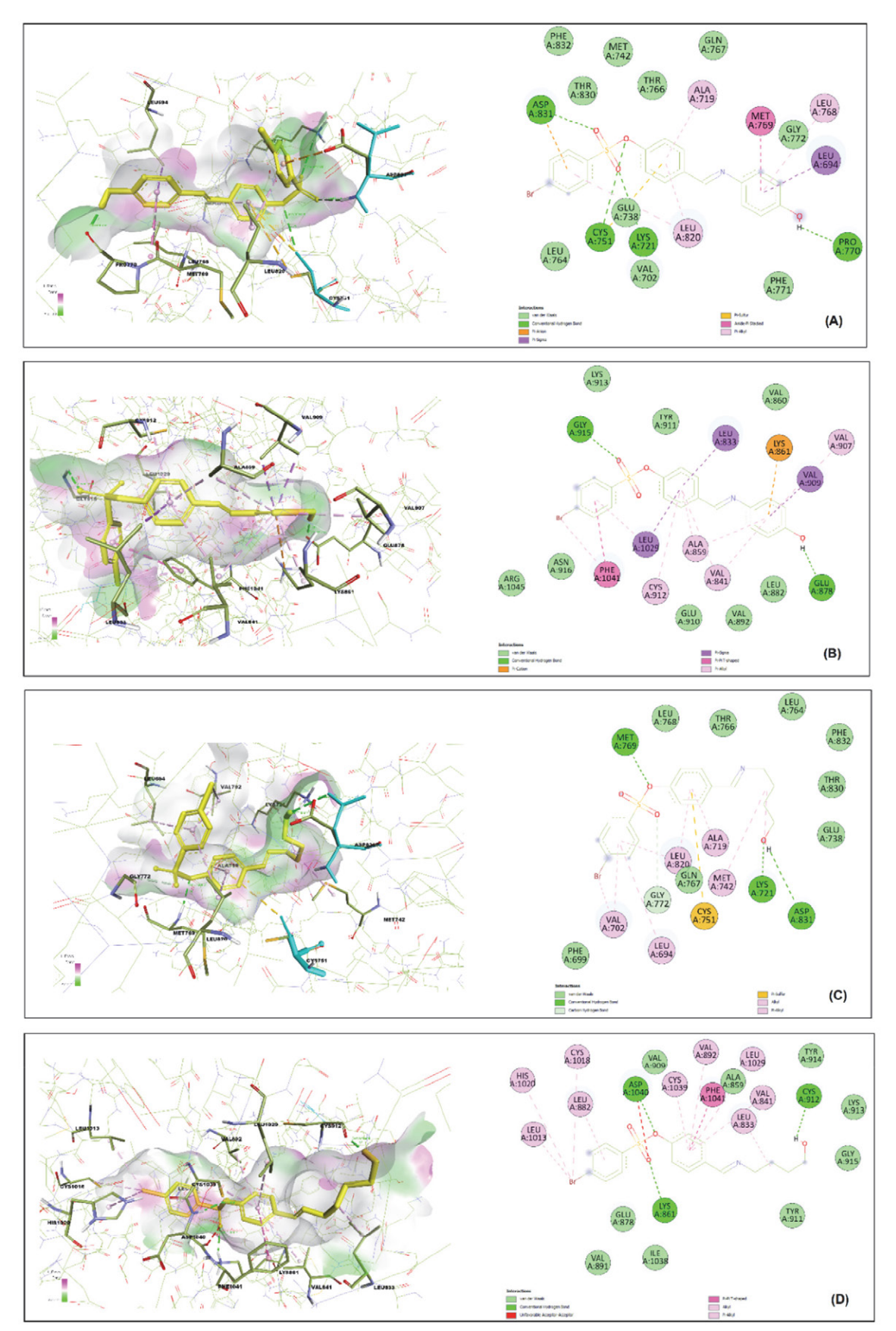
Hydrogen bond formation plays a critical role in ligand-protein stabilization, where both the number and type of hydrogen bonds significantly influence complex stability. Hydrogen bond furcation is prevalent in macromolecular structures, with hydrogen bond types, such as Pi-anion, Pi-sigma, Pi-Pi T-shaped, Pi-Pi stacking, and Pi-cation interactions, contributing to complex stability, which are typically characterized by bond lengths of >3.0 Å.<sup>46,47</sup>

In EGFR docking studies, compounds I and II displayed notable binding affinities with binding energies of -8.60 kcal/mol and -8.17 kcal/mol, respectively. The K<sub>i</sub> values for I (495.16 nM) suggest a stronger interaction than for II (1.02 µM), indicating a higher binding affinity of I for EGFR. Compared to the reference Erlotinib (binding energy of -7.69 kcal/mol and K<sub>i</sub> of 2.34 µM), both compounds I and II exhibit higher binding affinity. Both I and II formed multiple hydrogen bonds (4 each) with EG-FR, surpassing Erlotinib's three hydrogen bonds. Shared interactions with residues Leu694, Ala719, Lys721, Cys751, and Met769 indicate robust binding within the EGFR site, a stabilization pattern corroborated by previous kinase inhibitor studies. 48,49 Compound I displayed a unique hydrogen bond with Pro770 at a distance of 1.95 Å, and compound II exhibited its strongest bond with Lys721 at 1.67 Å. These specific interactions underscore compounds I and II's stability within EGFR, particularly through critical residues including Lys721. Additionally, unique contacts

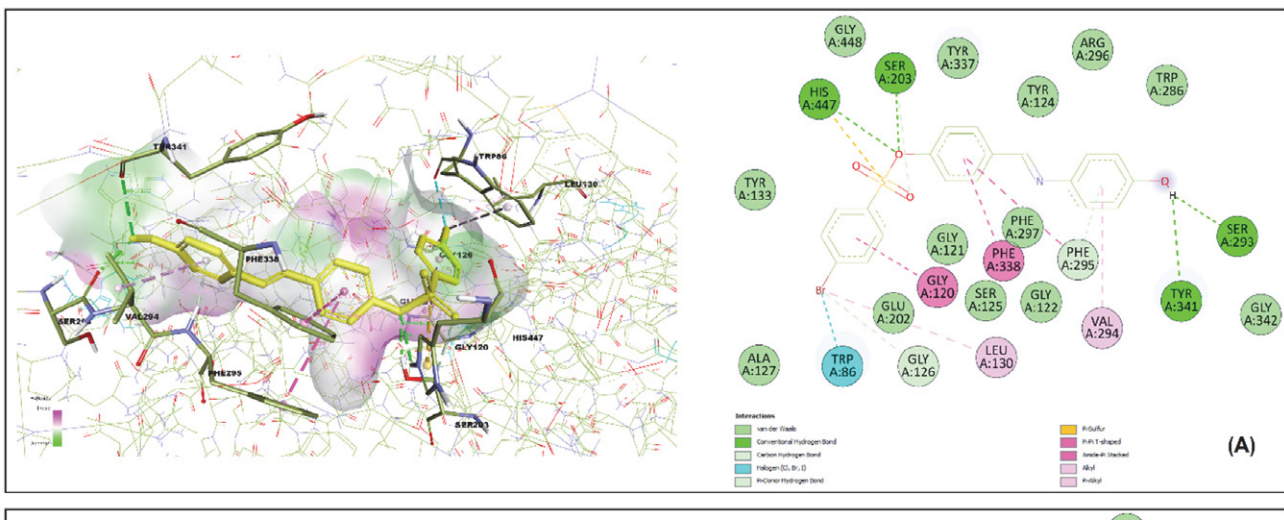
of compound I with Asp831 and compound II with Gly772 suggest slight conformational differences, potentially enhancing selectivity within the receptor binding pocket. The poses docked for compounds I, II, and reference molecules were evaluated, and the pose with the lowest binding free energy and inhibition constant was chosen (Table 8). Details regarding the interactions of the ligands are shown in Figure 6.

The docking results for VEGFR1 revealed that both compounds I and II displayed favorable binding energies and inhibition constants, making them competitive candidates alongside the reference molecules Dovitinib and Axitinib. Compound I, with a binding energy of -10.34 kcal/ mol and a K<sub>i</sub> of 26.24 nM, closely matched Axitinib, which had the highest binding affinity (binding energy of -10.65 kcal/mol, Ki of 15.05 nM) among all ligands tested. Compound II also showed a strong binding energy of -9.79 kcal/mol and a K<sub>i</sub> value of 67.13 nM, outperforming Dovitinib (binding energy of -8.73 kcal/mol,  $_{Ki} = 407.99$  nM). Key residues such as Leu833, Ala859, Lys861, and Cys912 were common interaction sites for all compounds, aligning with known critical interactions in VEGFR1 that stabilize ligand binding and influence the receptor's activation pathway. 45 Notably, compound I formed its strongest hydrogen bond with Glu878 at a bond length of 1.70 Å, while compound II's most effective bond was observed with Cys912, at a bond length of 1.67 Å. These specific, shortrange interactions likely contribute to the high binding affinity observed for both I and II, as similar short bond lengths have been associated with increased stability and specificity in ligand-receptor interactions. Furthermore, the additional hydrogen bonds formed by compound I with Gly915 and by compound II with Asp1040 suggest enhanced receptor-ligand stabilization within the VEG-FR1 binding site. This observation is particularly relevant for future structural optimization efforts, as hydrogen bonding at these positions has been associated with improved inhibitor efficacy in VEGFR1-targeted therapies.<sup>49</sup>

The binding energy and inhibition constant comparisons indicate that both compound I and compound II demonstrate profiles comparable to or surpassing those of established inhibitors Erlotinib<sup>50</sup> Dovitinib, and Axitinib.51 Notably, mol1's high affinity for both EGFR and VEG-FR1, akin to Axitinib, positions it as a promising candidate for dual-target applications, a strategy that may improve therapeutic outcomes in complex diseases such as cancer. The specific binding interactions of I and II with key residues in EGFR and VEGFR1 further underscore their potential as therapeutic candidates. Their distinct profiles, when compared to reference inhibitors, suggest effective kinase inhibition that could reduce receptor activity in pathways associated with tumor proliferation and angiogenesis. In conclusion, compounds I and II exhibit significant binding affinities for EGFR and VEGFR1, with interaction patterns that may contribute to their inhibitory effects. These findings validate the docking approach used



 $\textbf{Figure 6.} \ Docking \ poses \ of \ compound \ I \ 1 \ in \ the \ EGFR \ (1M17) \ binding \ pocket \ (A) \ and \ VEGFR-1 \ (3HNG) \ binding \ pocket \ (B), \ and \ of \ compound \ II \ in \ the \ EGFR \ (1M17) \ binding \ pocket \ (C) \ and \ VEGFR-1 \ (3HNG) \ binding \ pocket \ (D), \ displayed \ as \ 2D \ and \ 3D \ configurations.$ 



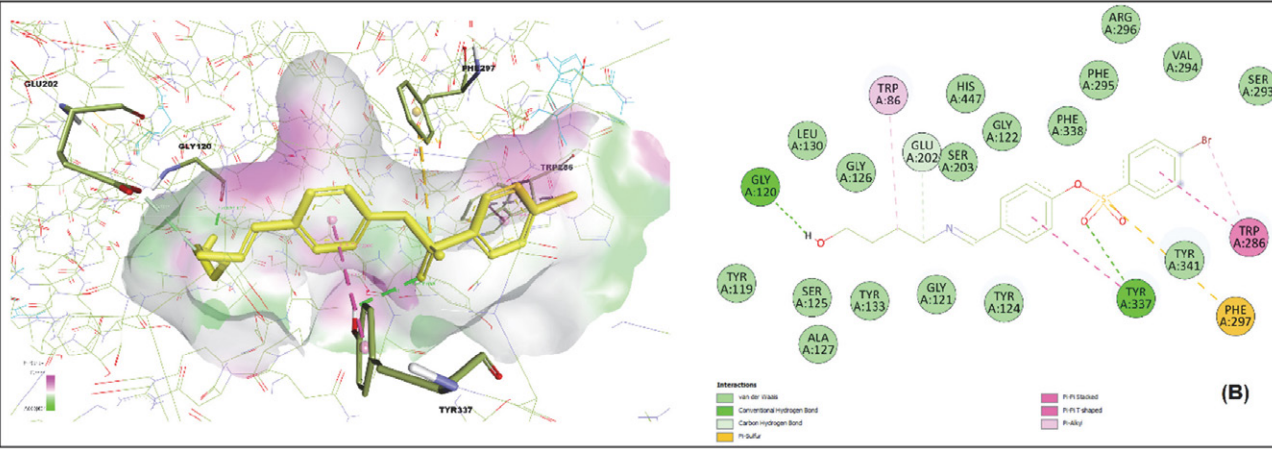


Figure 7. Docked structures visualized with BIOVIA Discovery Studio: 2D and 3D representations of Human Acetylcholinesterase complexes showing the best poses of compound I (A) and II (B) at the active site.

and highlight the potential of these compounds as leads for future drug design and development targeting EGFRand VEGFR1-associated pathways.

Human Acetylcholinesterase (AChE) plays a crucial role in the hydrolysis of the neurotransmitter acetylcholine, which is essential for synaptic transmission. Inhibition of AChE is an established strategy for treating diseases like Alzheimer's, where the regulation of acetylcholine levels is vital for cognitive function. Compounds that can effectively bind to AChE may offer potential therapeutic benefits in neurodegenerative disorders. <sup>52</sup>

Following the successful docking of compounds I and II with Human Acetylcholinesterase (AChE, PDB ID: 4M0E), significant binding interactions were observed, elucidating their potential as inhibitors. The 3D structure of AChE (PDB ID: 4M0E) utilized in this study has also been employed in similar docking analyses in the literature, highlighting its relevance in neurodegenerative research.  $^{53,54}$  Docking scores indicate a high binding affinity for compound I (binding energy of -10.71 kcal/mol,  $K_{\rm i}=14.16\,{\rm nM}$ ) compared to compound II, which demonstrates a slightly lower binding affinity (binding energy of -10.05

kcal/mol,  $K_i = 42.76$  nM). The reference molecule, Galantamine, displayed a less favorable binding energy of -9.33 kcal/mol and a higher  $K_i$  of 145.53 nM, suggesting that I and II are more effective AChE inhibitors by comparison.

Analysis of key molecular interactions reveals essential residues within the AChE binding pocket contributing to ligand stability and affinity. Both I and II engaged in critical hydrogen bonding interactions with Trp86 and Gly120, recognized for their roles in anchoring ligands within the AChE active site. 55 Compound I exhibited its strongest hydrogen bond with Ser293 at a bond length of 2.04 Å, while II's most effective bond was observed with Gly120 at a shorter distance of 1.85 Å. These strong interactions highlight the stability and affinity of I and II within AChE, with the short-range hydrogen bonds likely contributing to their enhanced inhibitory profiles.

Both compounds demonstrated interactions with several residues critical for AChE's catalytic function. For example, compound I exhibited binding interactions with Gly126, Leu130, Ser203, and His447, whereas compound II formed hydrogen bonds with Trp286 and Phe297. These distinct binding modes suggest that compound I may have

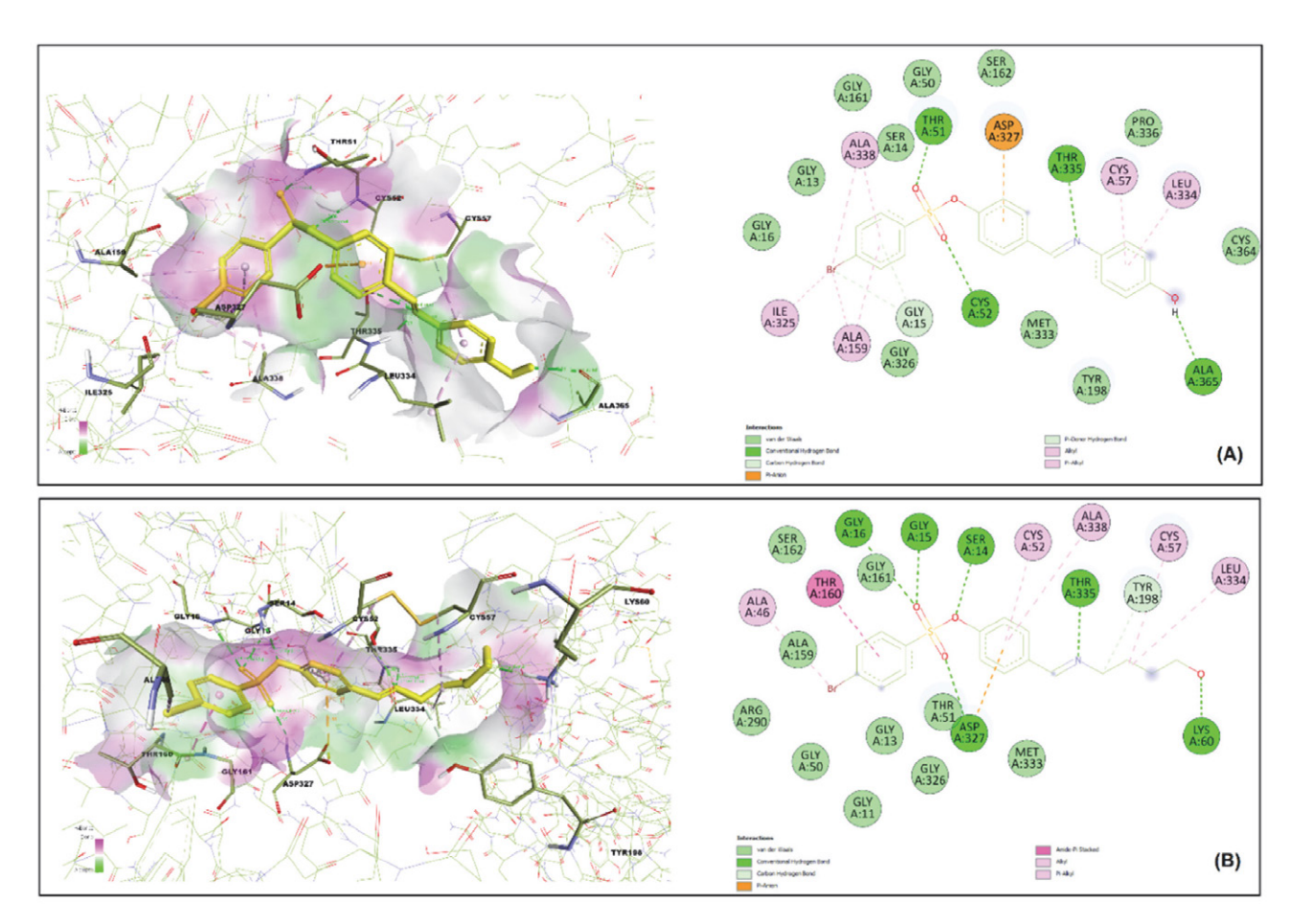


Figure 8. Visualization of compound I (A) and II (B) docked with Trypanothione Reductase (TRe) from *Leishmania infantum*, showing 2D and 3D representations of binding interactions and interacting residues within the enzyme's active site.

a slightly more stable binding configuration within the AChE active site, as it interacts with residues such as Ser203 and His447, known to play essential roles in AChE's active site conformation and catalytic efficiency.

The reference molecule, galantamine, exhibited some common binding interactions with compounds I and II, particularly with residues such as Trp86 and Phe338. However, the interactions of Galantamine primarily involved peripheral residues like Glu122 and Tyr124, potentially explaining its reduced affinity compared to I and II. This difference highlights the improved efficacy of I and II due to their more central interactions within the binding pocket.

In conclusion, both I and II demonstrate promising binding profiles as AChE inhibitors, with interaction patterns that underscore their potential efficacy within the enzyme's active site. Compound I's stronger binding affinity and specific hydrogen bonding with Ser293 may make it particularly suitable for further optimization in therapeutic design. Future studies may benefit from targeting additional interactions with residues like Tyr341 and Ser203 to further enhance stability and specificity. Details regarding the interactions of the ligands are shown in Figure 7.

Trypanothione Reductase (TRe) from *Leishmania infantum* is an essential enzyme involved in the detoxification of reactive oxygen species and is a critical target for anti-leishmanial drugs. By inhibiting TRe, it is possible to disrupt the redox balance within the parasite, leading to increased susceptibility to oxidative stress and ultimately, parasite death.<sup>56</sup> The 3D structure of TRe utilized in this study has also been used in similar docking analyses in the literature, underscoring its relevance in anti-leishmanial drug discovery efforts.<sup>57,58</sup>

The docking study conducted with Trypanothione Reductase (TR) from *Leishmania infantum* (PDB ID: 2JK6) highlights significant interactions and binding affinities for compounds I and II, with comparative insights against the reference compound Amphotericin B. The high binding affinity observed for I, with a binding energy of -11.15 kcal/mol and a  $K_i$  of 6.71 nM, indicates a potent inhibitory potential within the TR active site. II, on the other hand, exhibited a slightly weaker binding affinity (binding energy of -9.26 kcal/mol,  $K_i = 162.70$  nM), suggesting a reduced inhibitory potential relative to I. Amphotericin B, serving as the reference compound, displayed a lower binding affinity with a binding energy of

Table 8. Docking scores of I and II against target proteins.

Target Protein	Ligand	Binding Energy (kcal/mol)	K <sub>i</sub> value	No. of H-Bonds	No. of Closest Residues	Interacting Key Residues
Epidermal growth factor receptor (EGFR) 1M17,	mol1	-8.60	495.16 nM	4	10	Leu694, Ala719, Lys721, Cys751, Leu768, Met769, Pro770, Leu820, Asp831
(Res:2.60 Å, Chain:A)	mol2	-8.17	1.02 μΜ	4	8	Leu694, Val702, Ala719, Lys721, Met742, Cys751, Met769, Gly772, Leu820, Asp831
	Erlonitib*	-7.69	2.34 μΜ	3	9	Leu694, Val702, Ala719, Lys721, Met742, Leu764, Thr766, Gln767, Met769, Cyc773, Leu820
Vascular endothelial growth factor receptor 1	mol1	-10.34	26.24 nM	2	8	Leu833, Val841, Ala859, Lys861, Glu878, Val907, Val909, Cys912, Gly915, Leu1029, Phe1041
(VEGFR1), 3HNG (Chain:A, Res:2.70 Å)	mol2	-9.79	67.13 nM	3	9	Leu833, Val841, Ala859, Lys861, Leu882, Val892, Cys912, Leu1013, Cys1018, His1020, Leu1029, Cys1039, Asp1040, Phe1041
	Dovitinib*	-8.73	407.99 nM	2	8	Leu833, Ala859, Lys861, Glu878, Leu882, Val892, Val909, Tyr911, Cys912, Leu1029, Cys1039
	Axitinib*	-10.65	15.05 nM	3	8	Val841, Lys861, Glu878, Ile881, Leu882, Val891, Val892, Val907, Cys1018, Ile1038, Cys1039, Asp1040, Phe1041
Human Acetylcholi- nesterase, 4M0E (Res: 2.00 Å,	mol1	-10.71	14.16 nM	2	13	Trp86, Gly120, Gly126, Leu130, Ser203, Ser293, Val294, Phe295, Phe338, Tyr341, His447
Chain: A).	mol2	-10.05	42.76 nM	3	17	Trp86, Gly120, Trp286, Phe297, Tyr337
	Galantamine*	-9.33	145.53 nM	3	10	Trp86, Glu122, Tyr124, Phe338, His447
Trypanothione Reductase from <i>Leishmania</i> infantum, 2JK6 (Res:	e mol1	-11.15	6.71 nM	6	11	Gly15, Thr51, Cys52, Cys57, Ala159, Ile325, Asp327, Leu334, Thr335, Ala338, Ala365
2.95 Å, Chain A)	mol2	-9.26	162.70 nM	7	10	Ser14, Gly15, Gly16, Ala46, Cys52, Thr160, Tyr198, Asp327, Leu334, Thr335, Lys60, Ala38,
	Amphotericin B*	-8.46	624.25 nM	4	18	Val194, Ile285, Tyr221, Arg222, Phe230, Asn330, Arg331, Thr374

<sup>\*</sup>Reference drugs

-8.46 kcal/mol, highlighting the comparatively enhanced activity of I and II as TR inhibitors.

Key molecular interactions revealed specific residues within the TR active site critical for ligand stabilization and binding. I interacted extensively with residues Gly15, Thr51, Cys52, and Thr335, forming a network of six hydrogen bonds, an interaction profile that is consistent with ligands reported in the literature that exhibit high affinity within TR's active pocket. <sup>59</sup> In particular, Cys52 and Asp327 are residues known to play essential roles in the TR catalytic mechanism, and compound I's interaction with these residues likely enhances its binding stability and inhibitory efficacy.

Compound II, while forming seven hydrogen bonds, exhibited distinct binding characteristics, engaging with residues Ser14, Gly15, Gly16, and Ala46, which are situated at more peripheral positions relative to compound I's central binding residues. The interaction of II with Asp327 and Thr335, residues shared with compound I, indicates some similarity in binding orientation (n) to compound I, though the additional involvement of peripheral residues, such as Lys60 and Ala38, may account for its comparatively reduced binding energy.

When evaluated against Amphotericin B, both I and II exhibited superior binding affinity and  $K_i$  values. Amphotericin B, interacting with peripheral residues includ-

ing Val194, Ile285, Tyr221, and Phe230, displayed a binding energy of –8.46 kcal/mol. Notably, Amphotericin B did not engage with key catalytic residues like Cys52 or Asp327, which likely contributes to its weaker affinity within the TR binding pocket compared to I and II.

In summary, both compounds I and II demonstrate promising binding interactions within the TR active site, with compound 1 exhibiting the strongest binding profile due to its interaction with central and catalytically relevant residues. Compound II, while interacting with some of these critical residues, also interacts with peripheral residues, suggesting a different, potentially less stable binding orientation. These findings highlight the potential of compound I as a lead compound for TR inhibition in *Leishmania* treatment strategies. Details regarding the interactions of the ligands are shown in Figure 8.

#### 4. Conclusions

In this study, compounds I and II were investigated using both experimental techniques and quantum mechanical methods. Their structural parameters, vibrational properties, frontier molecular orbital energies, and electronic characteristics were thoroughly analyzed. The molecules were characterized by <sup>1</sup>H NMR, <sup>13</sup>C NMR, UV-Vis, and FT-IR spectroscopy. The HOMO and LUMO energy values were used to evaluate chemical hardness, softness, electronegativity, and electronic structure. The energy gap between the HOMO and LUMO orbitals serves as an indicator of molecular stability; a larger energy gap generally corresponds to a more stable and less reactive molecule. In addition to structural and spectroscopic properties, the electronic transitions of these Schiff base derivativesknown for their significant biological potential such as anticancer activity were also examined. Notable insights were obtained regarding reactive sites and charge delocalization within the molecules. Furthermore, the dipole moment, polarizability, and hyperpolarizability were calculated, indicating that the compounds exhibit nonlinear optical (NLO) properties. These findings suggest that the molecules possess promising application-oriented features for future studies.

Molecular docking studies were also conducted to investigate the interactions of compounds I and II with four receptor proteins: EGFR, VEGFR1, acetylcholinesterase, and *Leishmania infantum* trypanothione reductase. Binding energies and inhibition constants obtained from the docking simulations revealed key molecular interactions, offering valuable insights into the therapeutic potential of these Schiff base derivatives.

#### 5. References

 K. K. Phull, O. J. Hao, Ind. Eng. Chem. Res. 1993, 32, 1772– 1779. DOI: 10.1021/ie00020a035

- H. S. Tsai, Y. Z. Wang, J. J. Lin, W. F. Lien, Appl. Polym. Sci. 2010, 116, 1686–1693. DOI: 10.1002/app.31689
- K. Zhang, J. Helm, D. Peschel, M. Gruner, T. Groth, S. Fischer, *Polymer* 2010, 51, 4698–4705. DOI: 10.1016/j.polymer.2010.08.034
- R. Xing, X. He, S. Liu, H. Yu, Y. Qin, X. Chen, K. Li, R. Li, P. Li, Mar. Drugs 2015, 13, 3072–3090.

DOI: 10.3390/md13053072

 P. Seedevi, M. Moovendhan, S. Vairamani, A. Shanmugam, Int. J. Biol. Macromol. 2017, 99, 519–529.

**DOI:** 10.1016/j.ijbiomac.2017.03.012

- Q. Li, L. Qiu, W. Tan, G. Gu, Z. Guo, RSC Adv. 2017, 7, 42225– 42232. DOI: 10.1039/C7RA08244D
- M. Tan, H. Wang, Y. Wang, G. Chen, L. Yuan, H. Chen, J. Mater. Chem. B 2014, 2, 569–576. DOI: 10.1039/C3TB21358G
- N. R. Pires, P. L. Cunha, J. S. Maciel, A. L. Angelim, V. M. Melo, R. C. De Paula, J. P. Feitosa, *Polym.* 2013, *91*, 92–99.
   DOI: 10.1016/j.carbpol.2012.08.011
- J. Yang, K. Luo, D. Li, S. Yu, J. Cai, L. Chen, Y. Du, *Int. J. Biol. Macromol.* 2013, 52, 25–31.

**DOI:** 10.1016/j.ijbiomac.2012.09.027

- A. Jain, A. Gulbake, S. Shilpi, A. Jain, P. Hurkat, S. K. Jain, Ther. Drug Carrier Syst. 2013, 30, 91–181.
  - DOI: 10.1615/CritRevTherDrugCarrierSyst.2013005678
- Y. Ünver, T. Usta, F. Çelik, A. Aydın, H. İ. Güler, N. Süleymanoğlu, R. Ustabaş, K. İ. Bektaş, *J. Mol. Struct.* **2025**, *1319*, 139553. **DOI:** 10.1016/j.molstruc.2024.139553
- R. Ustabaş, F. Çelik, N. Süleymanoğlu, H. İ. Güler, F. Türkan,
   E. Oğuz, Y. Ünver, Russ. J. Phys. Chem. A 2024, 98, 707–719.
   DOI: 10.1134/S0036024424040204
- 13. M. J. Frisch, G. W. Trucks, H. B. Schlegel, G. E. Scuseria, M. A. Robb, J. R. Cheeseman, G. Scalmani, V. Barone, B. Mennucci, G. A. Petersson, H. Nakatsuji, M. Caricato, X. Li, H. P. Hratchian, A. F. Izmaylov, J. Bloino, G. Zheng, J. L. Sonnenberg, M. Hada, M. Ehara, K. Toyota, R. Fukuda, J. Hasegawa, M. Ishida, T. Nakajima, Y. Honda, O. Kitao, H. Nakai, T. Vreven, J. A. Montgomery Jr, J. E. Peralta, F. Ogliaro, M. Bearpark, J. J. Heyd, E. Brothers, K. N. Kudin, V. N. Staroverov, R. Kobayashi, J. Normand, K. Raghavachari, A. Rendell, J. C. Burant, S. S. Iyengar, J. Tomasi, M. Cossi, N. Rega, J. M. Millam, M. Klene, J. E. Knox, J. B. Cross, V. Bakken, C. Adamo, J. Jaramillo, R. Gomperts, R. E. Stratmann, O. Yazyev, A. J. Austin, R. Cammi, C. Pomelli, J. W. Ochterski, R. L. Martin, K. Morokuma, V. G. Zakrzewski, G. A. Voth, P. Salvador, J. J. Dannenberg, S. Dapprich, A. D. Daniels, O. Farkas, J. B. Foresman, J. V. Ortiz, J. Cioslowski, D. J. Fox, 2009. Gaussian 09 Revision A.1, Gaussian Inc., Wallingford, CT.
- R. Dennington, T. Keith, J. Millam, Semichem Inc, Shawnee Mission KS, GaussView, Version 5, 2009.
- R. Ditchfield, J. Chem. Phys. 1972, 56, 5688–5691.
   DOI: 10.1063/1.1677088
- K. Wolinski, F. F. Hinton, P. Pulay, J. Am. Chem. Soc. 1990, 112, 8251–8260. DOI: 10.1021/ja00179a005
- 17. K. Momma, F. Izumi. J. Appl. Crystallogr. 2011, 44, 1272–1276. DOI: 10.1107/S0021889811038970
- S. J. Rettig, J. Trotter. Can. J. Chem. 1977, 55, 3071–3075.
   DOI: 10.1139/v77-430

- J. Kohanoff, N. J. Gidapoulos, Density Functional Theory: Basic, New Trends and Application; John Wiley & Sons Ltd.: Chichester, UK, 2003.
- B. T. Gowda, K. Jyothi, J. Kozisek, H. Fuess, Z. Naturforsch.
   2003, 58A, 656659. DOI: 10.1016/j.saa.2010.09.017
- I. Yilmaz, N. B. Arslan, C. Kazak, K. Sancak, Y. Unver, *Acta Crystallogr. Sect. E* 2006, 62, o3067–o3068.
   DOI: 10.1107/S1600536806023981
- M. Li, X. Chen, Acta Crystallogr. Sect. E 2008, 64 o2349– o2349. DOI: 10.1107/S160053680803688X
- Y. Ünver, T. Usta, F. Çelik, A. Aydın, H. İ. Güler, N. Süleymanoğlu, K.İ. Bektaş, *J. Mol. Struct.* 2005, *1319*, 139553.
   DOI: 10.1016/j.molstruc.2024.139553
- J. P. Merrick, D. Moran, L. Radom, J. Phys. Chem. A 2007, 111, 11683–11700. DOI: 10.1021/jp073974n
- 25. R. M. Silverstein, F. W. Webster, Spectroscopic Identification of Organic Compounds, sixth ed., John Wiley & Sons, Inc., New York, 2003.
- R. Ustabaş, F. Çelik, N. Süleymanoğlu, H. İ. Güler, F. Türkan,
   E. Oğuz, Y. Ünver, Russ. J. Phys. Chem. A 2024, 98, 707–719.
   DOI: 10.1134/S0036024424040204
- D. Lin-Vien, N. B. Colthup, W. G. Fateley, J. G. Grasselli, The Handbook of Infrared and Raman Characteristic Frequencies of Organic Molecules. Academic Press, Boston, MA, 1991.
- D. Ramarajan, K. Tamilarasan, Z. Milanovic, D. Milenkovic,
   Z. Markovic, S. Sudha, E. Kavitha, J. Mol. Struct. 2020, 1205,
   127579. DOI: 10.1016/j.molstruc.2019.127579
- P. D. S. Babu, S. Periandy, S. Mohan, S. Ramalingam, B. G. Jayaprakash, *Spectrochim. Acta A* 2011, 78, 168–178.
   DOI: 10.1016/j.saa.2010.09.017
- M. A. Abbasi, A. Anum, S. Z. Siddiqui, M. Nazir, M. Ashraf,
   A. Noreen, S. A. A. Shah, *Pharm. Chem. J.* 2022, 56, 61–70.
   DOI: 10.1007/s11094-022-02598-y
- 31. N. M. O'Boyle, A. L. Tenderholt, K. M. Langner, *J. Comput. Chem.* **2008**, *29*, 839–845. **DOI:** 10.1002/jcc.20823
- R. Parthasarathi, V. Subramanian, D. R. Roy, P. K. Chattaraj, Bioorg. Med. Chem. 2004, 12, 5533–5543.
   DOI: 10.1016/j.bmc.2004.08.013
- 33. M. Evecen, G. Duru, H. Tanak, A. A. Ağar, *J. Mol. Struct.* **2016**, *1118*, 1–9. **DOI:** 10.1016/j.molstruc.2016.03.079
- 34. S. Muthu, J. U. Maheswari, T. Sundius, *Spectrochim. Acta A* **2013**, *106*, 299–309. **DOI**: 10.1016/j.saa.2012.12.080
- D. W. Schwenke, D. G. Truhlar, Systematic study of basis set superposition errors in the calculated interaction energy of two HF molecules. *J. Chem. Phys.* 1985, 82, 2418–2426.
   DOI: 10.1063/1.448335
- 36. M. Gutowski, J. van Duijneveldt-van de Rijdt, J. H. van Lenthe, F. B. van Duijneveldt, *J. Chem. Phys.* **1993**, *98*, 4728–4737. **DOI:** 10.1063/1.465106
- 37. M. Evecen, H. Tanak, *Appl. Phys. A* **2017**, *123*, 1–6. **DOI:** 10.1007/s00339-016-0693-4
- D. A. Kleinman, *Phys. Rev.* 1962, 126, 1977–1979.
   DOI: 10.1103/PhysRev.126.1977
- X. Y. Meng, H. X. Zhang, M. Mezei, M. Cui, Curr. Comput. Aided Drug Des. 2012, 7, 146–157.
   DOI: 10.2174/157340911795677602

- D. Chen, N. Oezguen, P. Urvil, C. Ferguson, S. M. Dann, T. C. Savidge, Sci. Adv. 2016, 2, e1501240.
   DOI: 10.1126/sciadv.1501240
- 41. C. Y. Goreci, *J. Mol. Struc.* **2022**, *1263*, 133149. **DOI:** 10.1016/j.molstruc.2022.133149
- 42. A. H. Abbas, A. A. R. Mahmood, L. H. Tahtamouni, Z. A. Al-Mazaydeh, M. S. Rammaha, F. Alsoubani, R. I. Al-bayati, *Pharmacia* **2021**, *68*, 679–692.
  - DOI: 10.3897/pharmacia.68.e70654
- 43. F. S. Tokalı, H. Şenol, Ş. Bulut, E. Hacıosmanoğlu-Aldoğan, *Journal of Molecular Structure*, **2023**, 1282, 135176. **DOI:** 10.1016/j.molstruc.2023.135176
- 44. H. Zhang, A. Berezov, Q. Wang, G. Zhang, J. Drebin, R. Murali, M. I. Greene, ErbB receptors: from oncogenes to targeted cancer treatmen. *J. Clin. Investig.* **2007**, *117*, 2051–2058. **DOI:** 10.1172/JCI32278
- 45. M. Shibuya, *Angiogenesis* **2006**, *9*, 225–230. **DOI:** 10.1007/s10456-006-9055-8
- 46. S. K. Panigrahi, G. R. Desiraju, *Proteins* **2007**, *67*, 128–141. **DOI:** 10.1002/prot.21253
- Z. B. Milanovic, Z. S. Markovic, D. S. Dimic, O. R. Klisuric,
   I. D. Radojevic, D. S. Sklic, E. H. Avdovic, *Comptes Rendus*.
   Chimie 2021, 24, 215–232. DOI: 10.5802/crchim.68
- 48. R. S. Herbst, *Int. J. Radiat. Oncol. Biol. Phys.* **2004**, *59*, 21–26. **DOI:** 10.1016/j.ijrobp.2003.11.041
- C. K. Lee, M. E. Lee, W. S. Lee, J. M. Kim, K. H. Park, T. S. Kim, K. Y. Lee, J. B. Ahn, H. C. Chung, S. Y. Rha, *Am. J. Cancer Res.* 2014, 5, 72–86.
- 50. C. M. Rocha-Lima, L. E. Raez, *P & T* **2009**, *34*, 554.
- 51. R. J. Kelly, O. Rixe, *Target Oncol.* **2009**, *4*, 297–305. **DOI:** 10.1007/s11523-009-0126-9
- M. Lane Roger, M. Kivipelto, N. Greig, *Clin. Neuropharmacol.* 2004, 27, 141–149.
  - **DOI:** 10.1097/00002826-200405000-00011
- Y. Ünver, N. Süleymanoğlu, R. Ustabaş, H. İ. Güler, E. Bektaş, K. İ. Bektaş, F. Çelik, *J. Ind. Chem. Soc.* 2022, 99, 100690.
   DOI: 10.1016/j.jics.2022.100690
- 54. N. Süleymanoğlu, F. Çelik, R. Ustabaş, H. İ. Güler, H. Şahin, Ş. Direkel, Y. Ünver, *Russ. J. Phys. Chem. A* 2023, 97, 3037–3049. DOI: 10.1134/S0036024423130162
- M. B. Colovic, D. Z. Krstic, T. D. Lazarevic-Pasti, A. M. Bondzic, V. M. Vasic, *Curr. Neuropharmacol.* 2013, *11*, 315–335.
   DOI: 10.2174/1570159X11311030006
- 56. J.Kuldeep, P. Kaur, N. Goyal, M. I. Siddiqi, *J. Biomol. Struct. Dyn.* **2021**, *39*, 960–969. **DOI**: 10.1080/07391102.2020.1721330
- N. Süleymanoğlu, Y. Ünver, R. Ustabaş, F. Çelik, H. İ. Güler, Ş. Direkel, K. İ. Bektaş, *J. Mol. Struct.* 2024, 1314, 138724.
   DOI: 10.1016/j.molstruc.2024.138724
- N. Süleymanoğlu, R. Ustabaş, H. İ. Güler, Ş. Direkel, F. Çelik,
   Y. Ünver, J. Biomol. Struct. Dyn. 2023, 41, 5970–5980.
   DOI: 10.1080/07391102.2022.2098825
- J. S. Berger, J. Hochman, I. Lobach, M. A. Adelman, T. S. Riles,
   C.B. Rockman, *J. Vasc. Surg.* 2013, 58, 673–681.
   DOI: 10.1016/j.jvs.2013.01.053

#### **Povzetek**

Pripravili smo derivate 4-bromobenzenesulfonata (I in II) in jih proučili s FTIR in NMR spektroskopskimi metodami ter s kvantno kemijskimi nračuni na podlagi teorije gostotnih funkcionalov (DFT). Ugotovili smo, da se skalirane vibracijske frekvence izračunane na nivoju B3LYP/6-311++G(d,p) ujemajo z eksperimentalno določenimi vrednostmi, kar potrjuje veljavnost izračunov. Za spojine smo pridobili optimizirane molekulske strukture, UV-Vis spektre in lastnosti nelinearnega optičnega odziva (NLO). Stabilnost molekul, ki izhaja iz hiper-konjugacijskih interakcij in delokalizacije naboja, smo analizirali z metodo naravnih veznih orbital (NBO). Izračunane energije HOMO in LUMO so pokazale, da v molekulah poteka znaten prenos naboja.

Poleg tega smo preučili interakcije med sintetiziranima spojinama I in II ter štirimi receptorji: EGFR, VEGFR1, acetilholinesterazo in trypanothione reduktazo Leishmania infantum. Molekulsko sidranje je omogočilo oceno energij vezave in inhibicijskih konstant ter razkrilo ključne interakcije, ki določajo terapevtski potencial obravnavanih spojin.



Except when otherwise noted, articles in this journal are published under the terms and conditions of the Creative Commons Attribution 4.0 International License